

TEM study of the FSW nugget in AA2195-T81

J.A. Schneider¹, A.C. Nunes, Jr.², P.S. Chen³, G. Steele³

¹Department of Mechanical Engineering,

Mississippi State University, Mississippi State, MS.

²Materials, Processes and Manufacturing of Metallic Materials,

NASA-Marshall Space Flight Center, Huntsville, Al.

³Morgan Research Corp., Huntsville, Al.

Abstract:

During friction stir welding (FSW) the material being joined is subjected to a thermal-mechanical process in which the temperature, strain and strain rates are not completely understood. To produce a defect free weld, process parameters for the weld and tool pin design must be chosen carefully. The ability to select the weld parameters based on the thermal processing requirements of the material, would allow optimization of mechanical properties in the weld region. In this study, an attempt is made to correlate the microstructure with the variation in thermal history the material experiences during the FSW process.

Keywords: friction stir welding, Al-Li alloy 2195, substructure, transmission electron microscopy.

Background

FSW is a solid-phase joining, or welding process that was invented in 1991 at The Welding Institute (TWI) [1]. The process is potentially capable of joining a wide variety of aluminum alloys that are traditionally difficult to fusion weld. The FSW process produces welds by moving a non-consumable rotating pin tool along a seam between work pieces that are firmly clamped to an anvil. At the start of the process, the rotating pin is plunged into the material to a pre-determined load. The required heat to soften the material is produced by a combination of deformation and frictional heating. The shape of the tool shoulder and supporting anvil promotes a high hydrostatic pressure along the joint line as the tool shears and literally stirs the metal together.

Several studies have been undertaken to measure the temperature in the weld nugget during friction stir welding [2-5]. Most involve embedding a thermocouple in the material near the weld centerline and relate temperatures approximately 0.8 times the absolute melting temperature in research on Al alloys. Although this provides a bulk temperature indication, variations within the weld zone cannot be quantified. The general weld temperature is determined by the weld parameters of tool travel and rotation speed. Additionally, the shoulder design of the pin tool may also contribute significantly to the heat input [2].

Many of the commercial aluminum alloys applicable for the FSW process are precipitation strengthened. Mechanical properties of FSW precipitation strengthened

alloys are strongly dependent on the size and distribution of the strengthening precipitates and only slightly on the grain size [6-11]. In some reported studies, a decrease in strength in the weld nugget and heat affected zone has been correlated with an overaging of the precipitates [7, 9, 10, 12]. In a study by Sutton, et. al. [13], alternating bands of precipitates were observed in the FSW wake, suggesting periodic variability in the thermal history. The ability to select the weld parameters based on the required heat treatment schedule for the solution-precipitation sequence of the aluminum alloys would improve the weld properties. In this study, TEM imaging of the FSW nugget in AA2195-T81 was compared with studies of time-temperature-precipitation (TTP) behavior [14-16] to assess the variation in the thermal history within the weld nugget.

Experimental Procedure

The material used in this study was an Al-Li-Cu alloy plate 2195-T8 that is 8.2 mm (0.323") thick. The nominal chemistry of this alloy is 4.19 wt.% Cu, 0.95 wt.% Li, 0.29 wt.% Mg, 0.31 wt. % Mg, 0.31 wt. % Ag, 0.12 wt. % Zr with the balance Al. Welding was performed using a tool with a 30.5 mm (1.2") diameter shoulder and a 12.7 mm (0.5") diameter right hand threaded pin approximately 7.9 mm (0.312") in length. The Al plates were aligned so that the weld tool traveled along the rolling direction of the plate material and penetrated through the normal direction of the processed plates.

Metallographic specimens were taken from the three orientations of the parent material as shown in Figure 1. The specimens were mounted, polished and viewed in the unetched

condition using light microscopy. The initial microstructure of the parent material (PM) shows the elongated pancake shaped grains typical of a rolled microstructure. Additional specimens taken from the cross section and transverse sections of the weld were also mounted, polished, and etched using Keller's Regent to document the macrostructure.

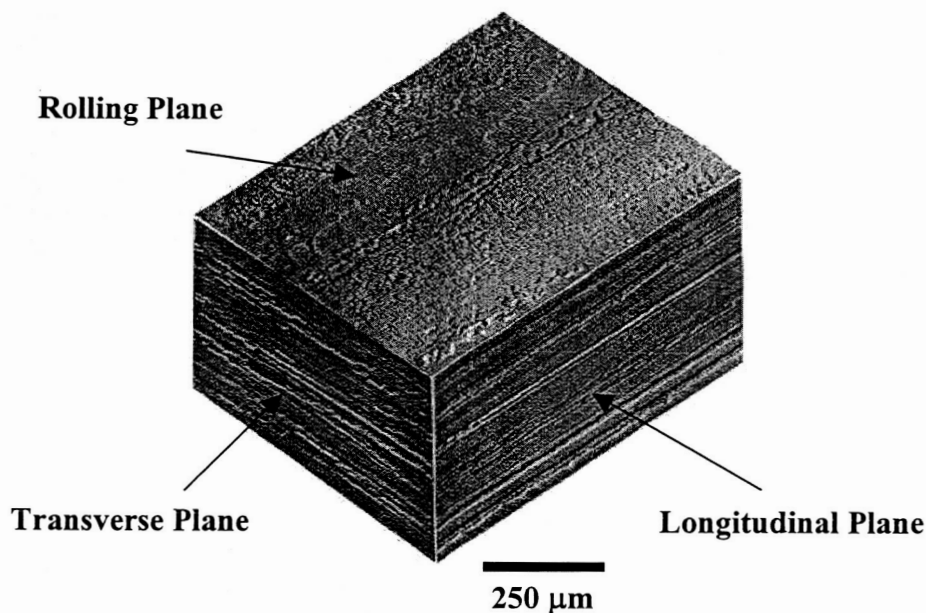


Figure 1. Optical microstructure of as-polished parent material (PM).

Thin foil specimens for the transmission electron microscope (TEM) images were obtained from the parent material (P) and center of the weld nugget (N) as shown in Figure 2. The specimens were mechanically ground to the desired thickness for microstructural examination in a JEOL JEM-2000 FE II TEM operated at 200 kV. The foils were twinjet electropolished to perforation at -20°C and 12 V in an electrolyte of 30% nitric acid in methanol. Precipitates were examined by the combined use of selected area diffraction (SAD) and bright field/dark field techniques. Matrix precipitates were

identified using an electron beam direction parallel to the Al $[110]_{\text{matrix}}$ and $[100]_{\text{matrix}}$ zone axis.

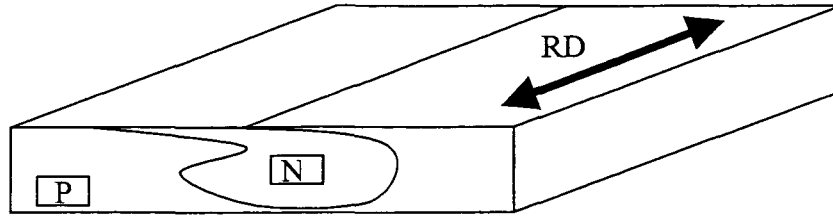


Figure 2. Location of TEM specimens for P – parent material specimens and N – FSW nugget specimens.

Rockwell B hardness measurements were made of the parent material and weld nugget. An average was recorded based on 6 measurements in regions similar to the TEM specimen location. Average values for the parent material was 90 ± 0.7 and in the FSW nugget was 67 ± 1.8 .

Results

The grains of the parent material are pancake shaped, typical of a rolled microstructure, as shown in the optical image in Figure 1 and TEM image in Figure 3. Aligned with the rolling direction, the major diameter is several millimeters long with a transverse width of $250 - 500 \mu\text{m}$. The thickness of the elongated grains is $2-4 \mu\text{m}$. Subgrain boundaries are

observed in the bright field image (BFI) of Figure 3, subdividing the elongated grains of the parent material.

Figure 4 is a bright field image (BFI) of a typical grain in the AA 2195-T81 parent material with a corresponding selected area diffraction pattern of the Al [110] zone axis. A reference selected area diffraction (SAD) pattern for Al matrix is shown in Figure 5a. Precipitates present in the Al matrix and identified by SAD are T_1 and θ' . Peak hardness for the T-8 temper is reported to be $H_{RB} = 95$ to 97 [17]. The T_1 (Al_2CuLi) primary strengthening phase is reported to form after extended artificial aging (>16 h) [16]. The θ' (Al_2Cu) secondary strengthening phase is reported to be present in all 2195 alloys, independent of the heat treatment conditions.

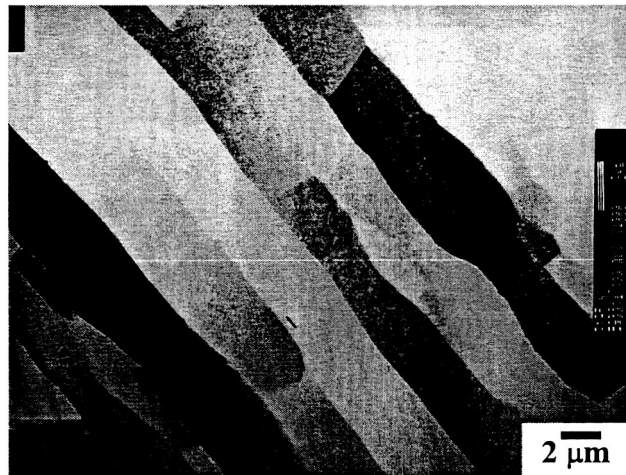


Fig. 3. TEM BFI of the elongated parent material grains and subgrain boundaries.

The θ' phase is reported to be tetragonal discs that are semi-coherent with the aluminum matrix [17]. Viewing the resulting diffraction of very fine, platelet morphologies give

rise to streak patterns in the Al matrix SAD. The θ' precipitates have been indexed in the Al $[110]$ zone axis as streaks in the short diagonal of the aluminum rhombus, as shown in Figure 5b. The T_1 is a hexagonal crystal structure with $(0001) T_1 \parallel \{111\} Al$ and $\langle 0101 \rangle T_1 \parallel \langle 110 \rangle Al$. Viewed in the Al $[110]$ zone axis, two variants of T_1 are inclined to the zone axis and produce spots that lie along the long diagonal of the Al SAD rhombus. The other 2 variants of the T_1 phase are parallel to the zone axis and produce streaks that form the sides of the Al SAD rhombus, as shown in Figure 5c.

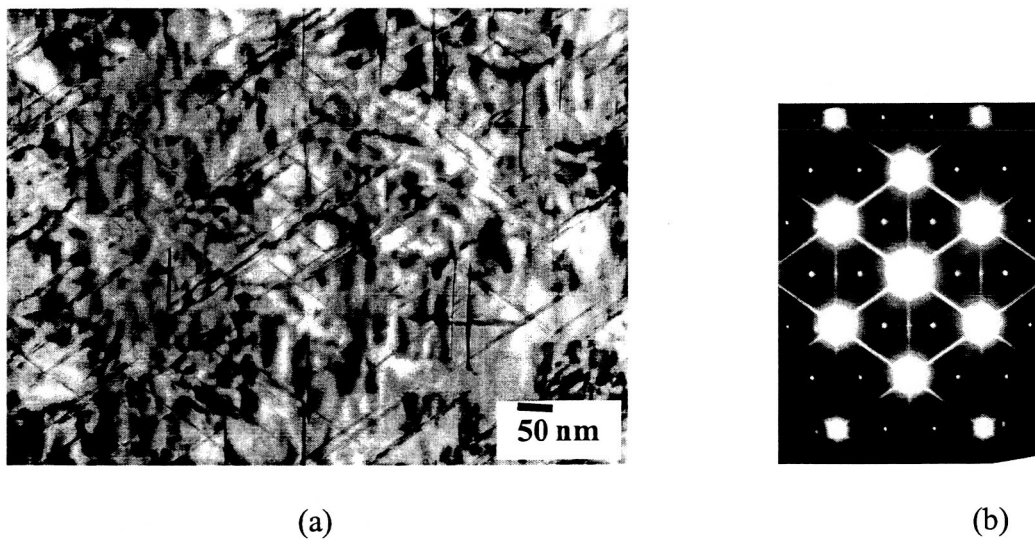


Fig. 4. Precipitates of θ' and T_1 in parent material (a) BFI and (b) SAD of (110) zone axis.

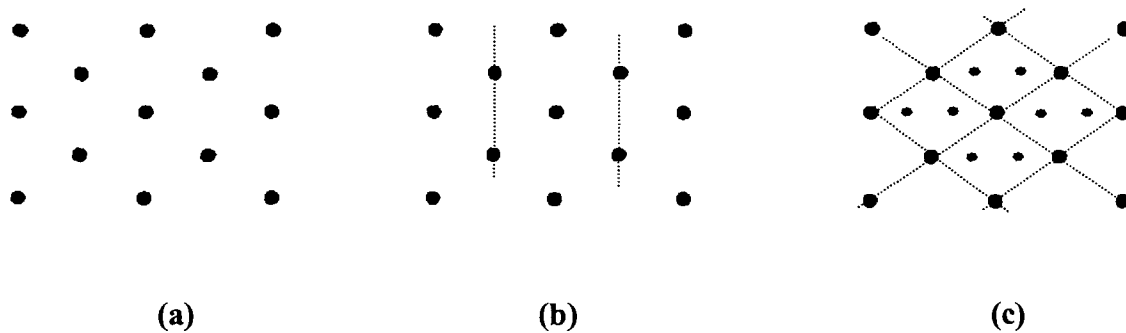
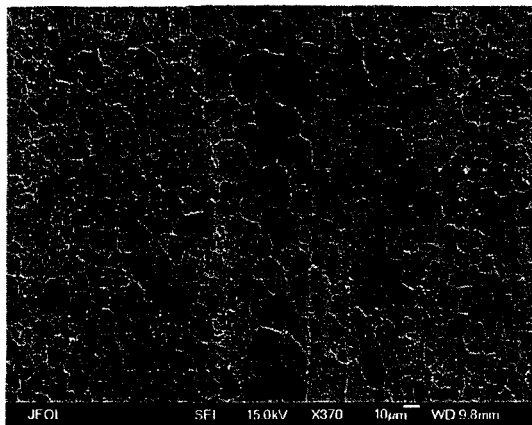


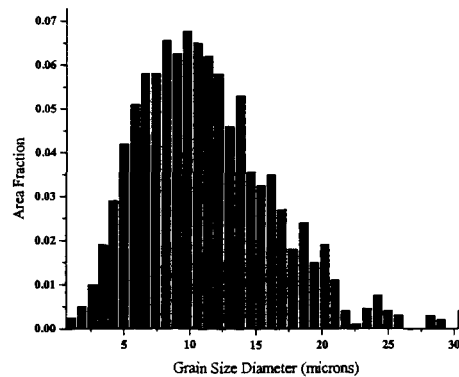
Fig. 5. (a) SAD pattern for the [110] zone axis of Al, (b) SAD pattern of [110] zone axis showing orientation of θ' precipitate streaks, and (c) SAD pattern of [110] showing orientation of T_1 precipitate streaks.

The T_1 phase precipitates in Figure 4 are approximately 60 to 115 nm long and 2-3 nm thick. At temperatures above 482° C, the precipitates in the AA2195 alloy are driven into solution instantaneously [16]. This is similar to the reported solutionizing temperature for Al-Li-Cu alloy AF/C489 [18].

A scanning electron microscopy (SEM) image is shown in Figure 6a for a section of the FSW nugget. Equiaxed grains are observed in the weld nugget due to geometric recrystallization that results during the thermal-mechanical processing of the FSW process. Grain size distribution was obtained using orientation image mapping (OIM), shown in Figure 6b. The average grain size in the weld nugget is 10 μm , approximately twice the thickness of the parent material grains.



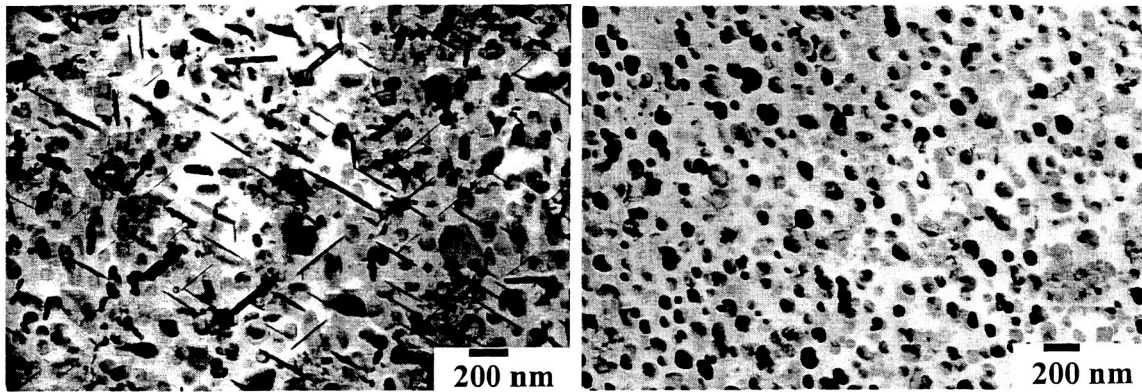
(a)



(b)

Fig. 6. (a) SEM image of weld nugget and (b) corresponding grain size distribution.

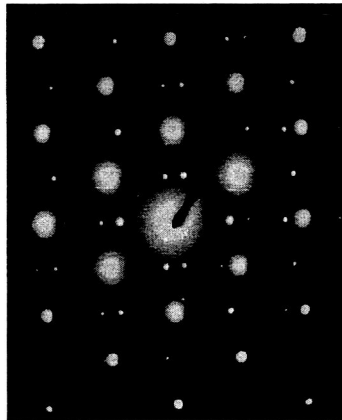
BFI's were taken of several grains in the center of the weld nugget zone. Two distinct distributions of precipitates were observed. Figure 7a shows a distribution of multiple phases, identified by SAD as θ' and T_1 , and T_B . The primary strengthening phase T_1 is much larger than those observed in the PM. T_1 precipitates are in the range of 200-300 nm long and 25-50 nm thick, indicating overaging. Adjacent grains in the weld nugget center, showed a distribution of a single phase, T_B , shown in Figure 7b. The T_B phase was identified by the SAD patterns in Figure 8a and 8b for the Al matrix [110] and [100] zone axis, respectively.



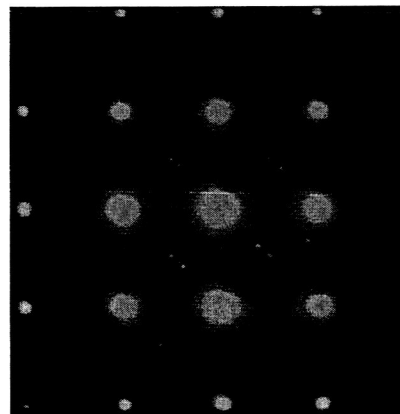
(a)

(b)

Fig. 7. Grains in the FSW nugget contain either (a) mixed precipitates of θ' , T_1 , and T_B or only (b) single T_B precipitates.



(a)



(b)

Fig. 8. SAD patterns of the (a) $[110]$ and (b) $[100]$ zone axis indexing the T_B precipitate shown in Figure 7b.

Discussion

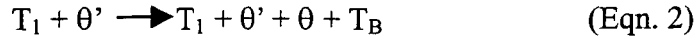
The initial hardness of the PM is near the reported peak aged properties for a microstructure with a primary T_1 and secondary θ' strengthening phases. Very little scatter was measured in the hardness reading of 90 ± 0.7 RHB, indicating a uniformity of microstructure in the grains averaged during the hardness test.

In contrast, a larger variation was measured in the hardness of the weld nugget. The variation of precipitation distribution in the grains within the same region of the weld nugget would agree with the non-uniform precipitation formation in the grains averaged for the hardness test measurements. Reported hardness values for grains with a mixture of overaged θ' , T_1 , and T_B phases is approximately 80 RHB and for grains with predominately T_B phase is approximately 20 RHB [16].

Figure 9 is a time-temperature-precipitation (TTP) diagram documenting the equilibrium precipitate formation sequences in the AA2195-T81 matrix of as-solutionized specimens [16]. Formation of the primary strengthening phase T_1 occurs around 800°F (427°C). The TTP diagram indicates the following steady state transformation sequence given in Eqn. 1.



Based on the phases present in Figure 7, the following transformation sequence is projected in Eqn. 2 for Figure 7a and Eqn. 3 for Figure 7b. The presence of the mixed precipitate phases in Figure 7a indicated either the temperature was not high enough or else the time was insufficient for complete transformation to T_B phase.



At low heat treat temperatures, in the range of 138-260 C, the T_1 phase predominates. Holding the material at temperatures within this range for short times (6 min) is reported to lead to coarsening of the T_1 phase [16]. Increasing the temperature to the range of 316 to 371° C, results in the rapid precipitation of θ and θ' (Al_2Cu). Following longer exposure (>10 h) at temperatures above 427° C, equiaxed precipitates of T_B ($\text{Al}_{7.5}\text{LiCu}_4$) form at the expense of T_1 , θ' and θ [16].

The TTP diagram shown in Figure 9 was obtained from equilibrium heat treatment studies using as-solutionized specimens, whereas the TEM specimens were prepared from 2195 that was peak aged and subsequently FSW'd. The variation in adjacent grains in the FSW nugget may indicate the grains in the nugget were subject to different thermal histories. Grains with predominant T_B phase indicated exposure to a higher temperature.

Previous studies on the precipitate distribution [7, 9, 10, 12] focused on the differences between the precipitation sequences across the macroscopic features of the weld zone. Strengthening precipitates in the PM were found to overage in the TMAZ and HAZ, and solutionize in the weld nugget. This was found to correlate with the hardness profiles measured across a transverse section of the weld nugget. These studies also indicated that the hardness in the weld nugget of precipitation strengthened alloys either increased or decreased depending on the weld parameters and the material welded. Studies on solution strengthened alloys reported no hardness variation across the weld transverse [19]. Microscopic examination of the variation with the same region of the weld nugget has not been reported in the literature, perhaps because of the lack of a model to explain the flow paths of the material during the FSW process. Recent publications [20, 21] suggest that two flow paths maybe present in the FSW process. Variation in the precipitate formation of the weld nugget supports this proposed model.

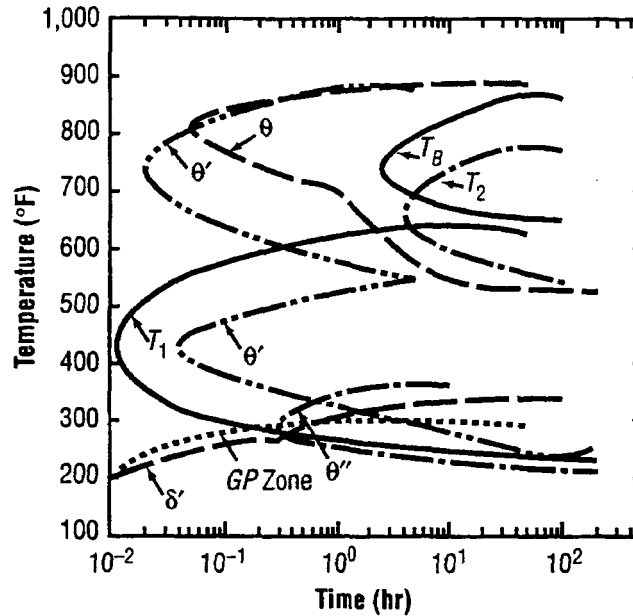


Fig. 9. Time-Temperature-Precipitation diagram for AA2195 [16].

Conclusions

TEM studies of the grains within the weld nugget indicate welding temperatures were obtained on the order of 400° C or higher during the FSW process. These temperatures are in agreement with published values for Al alloys indicating they are exposed to temperatures in the range of 400° to 450° C during FSWing [2, 7, 22]. Variations of the precipitates between adjacent grains indicates that there is a variation in the temperature within the weld nugget.

Degradation of strength in welds has been correlated with overaging of the precipitates in the matrix. Because FSW is a solid state joining process, the possibility of reducing the

strength due to overaging is reduced because the weld temperature can be controlled by the welding parameters.

Acknowledgements

One of the authors (JAS) acknowledges the support of the NASA-SFFP Grant No.

NAG8-1859

References.

1. THOMAS, W.M., et. al., 1991. Friction Stir Butt Welding, U.S. Patent No. 5,460,317.
2. TANG, W., et. al., *J. Mat. Proc. & Mfgt. Sci.* **7** (1998) 163.
3. CHEN, C.M., KOVACEVIC, R., *Int'l J. of Machine Tools and Manufacture* **43** [13] (2003) 1319.
4. MCCLURE, J.C., et. al., in Proc. 5th Int'l Conf. On Trends in Welding Research, Pine Mt., Georgia, June 1998, (ASM Intl, 1999) p. 590.
5. FRIGAARD, O., GRONG, O., MIDLING, O.T., *Met. & Mat. Trans.* **32A** (2001) 1189.
6. LIU, G., et. al., *Scripta Mater.* **37** (1997) 355.
7. MURR, L.E., LIU, G., MCCLURE, J.C., *J. Mat. Sci.* **33** [25] (1998) 1243.
8. MAHONEY, M.W., et. al., *Metall. & Mat. Trans.* **29A** (1998) 1955.
9. SATO, Y.S., et. al., *Metall. Mater. Trans.* **30A** (1999) 2429.
10. SATO, Y.S., et. al., *Metall. Mater. Trans.*, **30A** (1999) 3125.
11. JATA, K.V., SEMIATIN, S.L., *Scripta Mater.* **43** (2000) 743.
12. SATO, Y.S., KOKAWA, H., *Metall. and Mat. Trans.* **32A** (2001) 3023.
13. SUTTON, M.A., et. al., *Mat. Sci. & Engr.* **A323** (2002) 160.
14. BLANKENSHIP, JR., C.P., STARKE, JR., E.A., *Acta. Metall.* **42** (1994) 845.
15. CHEN, P.S., STANTON, W.P., NASA/TM 2002-211546 (2002).
16. CHEN, P.S., BHAT, B.N., NASA/TM 2002-211548 (2002).

17. PICKENS, J.R., KUMAR, K.S., BROWN, S.A., GAYLE, F.W., NASA Contractor Report #4368, (1991).
18. JATA, K.V., PANCHANADEESWARAN, S., VASUDEVAN, A.K., in Prod. of 1st National Seminar on the Application of Textures in Materials Research, Hyderabad, India, December 1997, ed. R.K. Ray, A.K. Singh, (Science Publishers, Inc., 1999) p. 161.
19. MURR, L.E., LIU, G., MCCLURE, J.C., *J. Mat. Sci. Letters* 16 (1997) 1801.
20. NUNES, JR., A.C., in Aluminum 2001: Proc. of 2001 TMS Annual Meeting Automotive Alloys and Joining Aluminum Symposia, Febr. 2001, ed. G. Kaufmann, J. Green, and S. Das, (TMS 2001) p. 235.
21. SCHNEIDER, J.A., NUNES, JR., A.C., in Friction Stir Welding and Processing II, March 2003, ed. K.V. Jata, M.W. Mahoney, R.S. Mishra, S.L. Semiatin, T. Lienert (TMS, 2003) p. 43.
22. SATO, Y.S., et. al., *Metall. & Mat. Trans.* 33A (2002) 625.

Figure Legends

Figure 1. Optical microstructure of as-polished parent material (PM).

Figure 2. Location of TEM specimens for P – parent material specimens and N – FSW nugget specimens.

Fig. 3. TEM BFI of the elongated parent material grains and subgrain boundaries.

Fig. 4. Precipitates of θ' and T_1 in parent material (a) BFI and (b) SAD of $[110]$ zone axis.

Fig. 5. (a) SAD pattern for the $[110]$ zone axis of Al., (b) SAD pattern of $[110]$ zone axis showing orientation of θ' precipitate streaks, and (c) SAD pattern of $[110]$ showing orientation of T_1 precipitate streaks.

Fig. 6. (a) SEM image of weld nugget and (b) corresponding grain size distribution.

Fig. 7. Grains in the FSW nugget contain either (a) mixed precipitates of θ' , T_1 , and T_B or only (b) single T_B precipitates.

Fig. 8. SAD patterns of the (a) $[110]$ and (b) $[100]$ zone axis indexing the T_B precipitate shown in Figure 7b.

Fig. 9. Time-Temperature-Precipitation diagram for AA2195 [16].